Multi-kingdom gut microbiota dysbiosis is associated with the development of pulmonary arterial hypertension

Yihang Chen,[a,b,i] Zhenzhen Chen,[c,i] Lirong Liang,[d,e,i] Jifeng Li,[d,i] Liukun Meng,[f] Wen Yuan,[a] Boqia Xie,[b] Xun Zhang,[g] Lin Feng,[a,e] Yanxiong Jia,[b,h] Zhou Fu,[b,h] Pixiong Su,[b,h] Zhaohui Tong,[d,*] Jiuchang Zhong,[b,**] and Xiaoyan Liu[a,b,***]

[a]Medical Research Center, Beijing Institute of Respiratory Medicine and Beijing Chao-Yang Hospital, Capital Medical University, Beijing, 100020, China
[b]Heart Center and Beijing Key Laboratory of Hypertension, Beijing Chao-Yang Hospital, Capital Medical University, Beijing, 100020, China
[c]Beijing Anzhen Hospital of Capital Medical University and Beijing Institute of Heart Lung and Blood Vessel Diseases, Beijing, 100029, China
[d]Department of Respiratory and Critical Care Medicine, Beijing Institute of Respiratory Medicine and Beijing Chao-Yang Hospital, Capital Medical University, Beijing, 100020, China
[e]Department of Clinical Epidemiology, Beijing Institute of Respiratory Medicine and Beijing Chao-Yang Hospital, Capital Medical University, 100020, Beijing, China
[f]Fuwai Hospital, Chinese Academy of Medical Sciences and Peking Union Medical College, State Key Laboratory of Cardiovascular Disease, National Center for Cardiovascular Diseases, Beijing, 100037, China
[g]Department of Pharmacy, Chinese PLA General Hospital, 100039, Beijing, China
[h]Department of Cardiac Surgery, Beijing Chao-Yang Hospital, Capital Medical University, Beijing, 100020, China

eBioMedicine
2025;115: 105686
Published Online xxx
https://doi.org/10.1016/j.ebiom.2025.105686

Summary

Background Gut microbiota dysbiosis has been implicated in pulmonary arterial hypertension (PAH). However, the exact roles and underlying mechanisms of multi-kingdom gut microbiota, including bacteria, archaea, and fungi, in PAH remain largely unclear.

Methods The shotgun metagenomics was used to analyse multi-kingdom gut microbial communities in patients with idiopathic PAH (IPAH) and healthy controls. Furthermore, fecal microbiota transplantation (FMT) was performed to transfer gut microbiota from IPAH patients or monocrotaline (MCT)-PAH rats to normal rats and from normal rats to MCT-PAH rats.

Findings Gut microbiota analysis revealed substantial alterations in the bacterial, archaeal, and fungal communities in patients with IPAH compared with healthy controls. Notably, FMT from IPAH patients or MCT-PAH rats induced PAH phenotypes in recipient rats. More intriguingly, FMT from normal rats to MCT-PAH rats significantly ameliorated PAH symptoms; restored gut bacteria, archaea, and fungi composition; and shifted the plasma metabolite profiles of MCT-PAH rats toward those of normal rats. In parallel, RNA-sequencing analysis demonstrated the expression of genes involved in key signalling pathways related to PAH. A panel of multi-kingdom markers exhibited superior diagnostic accuracy compared with single-kingdom panels for IPAH.

Interpretation Our findings established an association between multi-kingdom gut microbiota dysbiosis and PAH, thereby indicating the therapeutic potential of FMT in PAH. More importantly, apart from gut bacteria, gut archaea and fungi were also significantly associated with PAH pathogenesis, highlighting their indispensable role in PAH.

Funding This work was supported by Noncommunicable Chronic Diseases-National Science and Technology Major Projects No. 2024ZD0531200, No. 2024ZD0531201 (Research on Prevention and Treatment of Cancer, Cardiovascular and Cerebrovascular Diseases, Respiratory Diseases, and Metabolic Diseases), the National Natural Science Foundation of China of China (No. 82170302, 82370432), Financial Budgeting Project of Beijing Institute of Respiratory Medicine (Ysbz2025004, Ysbz2025007), National clinical key speciality construction project Cardiovascular

*Corresponding author.
**Corresponding author.
***Corresponding author. Medical Research Center, Beijing Institute of Respiratory Medicine and Beijing Chao-Yang Hospital, Capital Medical University, Beijing, 100020, China.
E-mail addresses: tongzhaohuicy@sina.com (Z. Tong), jczhong@mail.ccmu.edu.cn (J. Zhong), lxycyyy@mail.ccmu.edu.cn (X. Liu).
[i]These authors contributed equally to this study.

Surgery, Reform and Development Program of Beijing Institute of Respiratory Medicine (Ggyfz202417, Ggyfz202501), Clinical Research Incubation Program of Beijing Chaoyang Hospital Affiliated to Capital Medical University (CYFH202209).

Keywords: Pulmonary arterial hypertension; Gut microbiota; Metabolomics; Metagenomics; Fecal microbiota transplantation

Research in context

Evidence before this study

Previous research has suggested a link between gut microbiota dysbiosis and pulmonary arterial hypertension (PAH). However, despite evidence supporting the involvement of gut bacteria in PAH pathogenesis, the comprehensive role and mechanisms of multi-kingdom gut microbiota including bacteria, fungi, and archea in PAH remain poorly understood.

Added value of this study

This study expands and enriches current knowledge by revealing that multi-kingdom gut microbiota, including bacteria, archaea, and fungi, are collectively associated to the pathogenesis of PAH. Our findings indicate that in addition to gut bacteria, gut archaea and fungi are significantly altered in patients with idiopathic PAH. Furthermore, we highlight the therapeutic potential of fecal microbiota transplantation (FMT) in reversing PAH phenotypes. More attention should be paid to new insights into the microbial underpinnings of PAH and the therapeutic potential of targeted multi-kingdom microbiota–based interventions.

Implications of all the available evidence

Our findings highlight the critical need to move beyond a bacteria-centric view of gut microbiota in PAH, underscoring the relevance of a broader microbial landscape in the prevention and treatment of PAH.

Introduction

Pulmonary arterial hypertension (PAH) is a debilitating condition characterized by heightened resistance in the pulmonary vasculature, which leads to right-sided heart failure and potentially fatal outcomes if left untreated.[1] Among the various forms of PAH, idiopathic PAH (IPAH) represents a particularly challenging subset due to its unknown aetiology and poor prognosis.[2] Moreover, the underlying mechanisms driving IPAH remain poorly understood, which poses significant challenges for effective treatment and management. There is emerging evidence suggesting a potential link between gut microbiota (GM) imbalance and PAH, highlighting the gut–lung axis as a novel area of investigation in IPAH research.[3]

GM comprise not only bacteria but also fungi and archaea—all of which are fundamental to human health and disease.[4–6] Gut fungi and archaea contribute to cardiovascular diseases by metabolic pathways, immune responses, and systemic inflammation.[6–8] There is growing evidence of notable changes in the structure and function of gut bacterial community in PAH patients, including the enrichment of bacteria involved in trimethylamine N-oxide and purine metabolism and a reduction in butyrate- and acetate-producing bacteria.[9,10] Specific bacterial species in the gut correlate with PAH severity and clinical metrics, while patients with chronic thromboembolic pulmonary hypertension (CTEPH) show reduced alpha diversity and increased inflammatory markers.[11] Additionally, patients with PAH have lower levels of anti-inflammatory short-chain fatty acid (SCFA) genes and higher proinflammatory gene copies, along with altered plasma metabolite levels.[12] Animal studies support these findings, demonstrating changes in gut bacterial microbiota in PAH models, such as increased Firmicutes/Bacteroidetes ratios and gut pathology in rats with monocrotaline (MCT)-induced PAH, including increased gut permeability and microbial community shifts.[13–15]

Despite growing interest in the GM–PAH link, significant research gaps remain. Current studies primarily focus on bacterial components, with limited attention paid to the roles of gut fungi and archaea. Additionally, the association between GM and PAH remains unclear, considering that most of the existing studies are observational. There is also a lack of research on the effectiveness of fecal microbiota transplantation (FMT) in the treatment of PAH, particularly concerning how gut microbial communities, including bacteria, fungi, and archaea, may influence disease progression and therapeutic outcomes.

In this study, we performed multi-kingdom analyses of gut bacteria, archaea, and fungi in IPAH using both human and animal models. FMT was performed to assess whether GM from IPAH patients or MCT-PAH rats could induce phenotypic changes in recipient rats, thereby establishing a potential link between GM and PAH. Additionally, the therapeutic potential of FMT

in modulating PAH phenotypes was explored in rat models, providing insights for potential therapeutic applications. Finally, multi-kingdom microbial species with high diagnostic potential for IPAH were identified.

Methods

Ethics statement

Written informed consent was obtained from all participants before clinical data and biospecimen collection. The study received ethical approval from the Ethics Committees of Beijing Chao-Yang Hospital of Capital Medical University (approval No. 2023-ke-726). All animal experiments were followed ethical standards established by the Animal Experimentation Ethics Committee of Capital Medical University, Beijing, China (AEEI-2022-011), and adhered to current NIH guidelines for animal welfare and experimental protocols.

Study cohorts

Thirty-one patients diagnosed with IPAH were enrolled at Beijing Chao-Yang Hospital of Capital Medical University between November 2023 and August 2024. Diagnosis followed standard criteria from recent guidelines. Exclusion criteria were as follows: 1) age outside the range of 18–70 years; 2) positive response to acute pulmonary vasodilator testing via right-sided heart catheterization; 3) significant comorbidities such as coronary artery disease, pneumonia, diabetes mellitus, or chronic kidney disease; 4) family medical history of autoimmune diseases, cancer, or other severe heritable diseases; and 5) recent use of antibiotics within the last 3 months. Thirty-one age- and gender-matched healthy controls (HCs) were also recruited.

Animals

Sprague–Dawley (SD) rats, aged 5 weeks and weighing between 180 and 210 g, were procured from Beijing Vital River Laboratory Animal Technology Co., Ltd. The rats were housed under specific pathogen-free (SPF) conditions at Beijing Chao-Yang Hospital. They were kept under a 12-h light/dark cycle at a controlled temperature of 25 °C, with unrestricted access to food and water. The rats from each group were housed in separate cages to prevent cross-group interference. Additionally, the cages were cleaned regularly.

Human stool transfer in rats

Fecal donors were sourced from the human study cohorts. Fresh fecal samples were collected, homogenized with an appropriate amount of sterile precooled physiological saline, and thoroughly mixed. The mixture was filtered through a sieve to remove large particles and then transferred to centrifuge tubes. The samples were centrifuged at 3000 rpm for 20 min at 4 °C. The supernatant was discarded, and the pellet was weighed. An equal volume of precooled glycerol (20% of the bacterial pellet volume) was added to the pellet. The mixture was aliquoted into 15-mL centrifuge tubes, with 5 mL per tube, and stored at –80 °C.

The recipient rats were orally given antibiotics (metronidazole 200 mg/kg, vancomycin 100 mg/kg, neomycin sulphate 200 mg/kg, and ampicillin 200 mg/kg, J&K Scientific, Cat# 274 238, Cat# 122 263, Cat# 557 926, Cat# 290 395) once a day for four consecutive days to deplete the GM. The bacterial suspension was administered via oral gavage once daily for two weeks. The rats receiving FMT from HCs were designated as the HTN group (n = 6), while those receiving FMT from IPAH patients were designated as the PTN group (n = 6). Eight weeks after FMT, echocardiography was performed, followed by anaesthesia with pentobarbital sodium (40 mg/kg, Sigma–Aldrich, Cat# P3761) and sacrifice for haemodynamic measurements.

Rat stool transfer in rats

Following acclimation in a controlled environment, PAH was induced in rats by intraperitoneal administration of MCT at 60 mg/kg (Sigma–Aldrich, Cat# C2401). MCT powder was dissolved in a solution of ethanol and saline (2:8 ratio). The rats were randomly divided into the control (CON) group, which received a solvent injection, and the MCT-PAH (MCT) group, which received an MCT injection. For the rats receiving FMT, the bacterial suspension was obtained from 10 g of fresh fecal samples collected every morning from rats in the CON and MCT groups using sterile tubes. The fecal samples were homogenized with 20 mL of pre-cooled sterile normal saline for 1 min, followed by centrifugation at 1000 rpm for 5 min at 4 °C.

Before FMT, the recipient rats were orally given antibiotics (vancomycin 100 mg/kg, neomycin sulphate 200 mg/kg, metronidazole 200 mg/kg, and ampicillin 200 mg/kg, J&K Scientific, Cat# 274 238, Cat# 122 263, Cat# 557 926, Cat# 290 395) once daily for 4 days to deplete the GM. Each rat in the NTN group received gastric gavage of 2 mL of the fecal supernatant from the CON group for 14 consecutive days (n = 5). Simultaneously, each rat in the MTN group received gastric gavage of 2 mL of the fecal supernatant from the MCT group for 14 consecutive days (n = 9). Eight weeks after FMT, echocardiography was performed. Subsequently, the rats were anesthetized with pentobarbital sodium (40 mg/kg, Sigma–Aldrich, Cat# P3761) and sacrificed for haemodynamic measurements.

Fecal microbiota transplantation therapy

The rats were randomly divided into two groups, namely the CON group (n = 6), which received a solvent injection, and the MCT group (n = 12), which received an MCT injection. Subsequently, the MCT group was

further randomized into the MCT group and the normal-transplant microbiota (NTM) group (n = 6), with the NTM group receiving FMT from the CON group. Fresh fecal samples (10 g) were collected daily from the CON group and immediately mixed with 20 mL of pre-cooled sterile normal saline. Afterward, the mixture was subjected to centrifugation at 1000 rpm for 5 min at 4 °C. The supernatant was then carefully harvested for subsequent experimental procedures. Each rat in the NTM group received gastric gavage of 2 mL of the fecal supernatant from the CON group for 21 consecutive days.

Echocardiography was performed four weeks after MCT injection, followed by anaesthesia with pentobarbital sodium (40 mg/kg, Sigma–Aldrich, Cat# P3761) and sacrifice for haemodynamic measurements.

Echocardiography

Echocardiography assessment was conducted pursuing a previously described protocol.[16,17] An expert operator conducted echocardiography using a Visual Sonics VEVO 2100 system. The assessment of right ventricle (RV) function included measurements of tricuspid annular plane systolic excursion (TAPSE), RV free wall thickness (RVWT), RV end-diastolic dimension (RVEDD), and pulmonary artery acceleration time (PAAT). Data from three consecutive heartbeats were collected to normalize variations.

Haemodynamic measurements and tissue processing

Following echocardiographic assessment, RV systolic pressure (RVSP) was measured by right-sided heart catheterization. The hearts and lungs were then extracted and weighed. The weights of the RV free wall and the left ventricle (LV) plus septum (S) were measured, and the RV/(LV + S) ratio was calculated.

Histological examination

Lung tissues were soaked in 10% neutral buffered formalin solution for 72 h, embedded in paraffin, and sectioned into 4-μm-thick slices. Vascular remodelling was assessed by staining the cross-sections with Elastica-van Gieson (EVG) and haematoxylin and eosin (HE). A total of 40–60 intra-acinar vessels (<100 μm) were categorized as nonmuscular (NPA), partially muscular (PPA), or muscular (MPA) to evaluate the degree of muscularization. Muscularization was expressed as the proportion of NPA, PPA, and MPA to the total number of vessels.

Quantification of pulmonary vascular remodelling

EVG staining was used to assess the pulmonary artery media thickness and measure pulmonary arterial remodelling. The degree of muscularization was determined by two independent blinded examiners, with inter-person variability less than 10%. Obstruction level in pulmonary vessels (<100 μm) was calculated using the following equation: (area of outer vessel – area of inner vessel)/area of outer vessel. Pulmonary arterial vessels were categorized based on their external diameter into small pulmonary arterioles (<50 μm) and medium pulmonary arteries (>50 μm). Values from four randomly selected vessels per animal that generally exhibited round or oval shapes were measured and averaged.

Metagenomic sequencing

Total DNA was extracted using cetyltrimethylammonium bromide (CTAB) and sequenced by Oriental Yeekang (Beijing, China) Medicine Technology Co., Ltd. on the Illumina Novaseq 6000 platform, generating 2 × 150-bp paired-end reads. The quality of the extracted DNA was evaluated using NanoDrop spectrophotometry (Thermo Fisher Scientific), Qubit 2.0 fluorometer (Invitrogen), and agarose gel electrophoresis (AGE). The raw sequencing data were used for bioinformatics analyses.

Sequence taxonomic annotation

Metagenomic-sequencing datasets underwent quality-filtering with Trimmomatic v0.33 software to eliminate low-quality sequences. Human sequences were excluded using Bowtie2 v2.2.4 with the hg38 database. The remaining high-quality clean reads were used for downstream analyses. Bacterial and archaeal species were identified using MetaPhlAn4 (version 4.0.6, released on March 1, 2023). Concurrently, fungal species identification was performed using Kraken2 software (version 2.1.1). For both tools, default parameters were applied, and relative abundances of taxa were calculated at multiple taxonomic levels (phylum, class, order, family, genus, and species).

Microbial diversity and differential abundance analysis

Alpha diversity, including Shannon and Chao1 indexes, was calculated to assess microbial richness and diversity within each sample. Beta diversity was evaluated using Bray–Curtis dissimilarity and visualized through principal coordinate analysis (PCoA). Statistical significance of differences in beta diversity among groups was tested using PERMANOVA (adonis function in the vegan R package). Differentially abundant taxa between the experimental groups were identified using linear discriminant analysis effect size (LEfSe).

Metabolomics

Blood samples collected in ethylene diamine tetra-acetic acid (EDTA) vacutainer tubes were centrifuged at 3000 rpm for 10 min and stored at –80 °C for liquid chromatography–mass spectrometry (LC-MS) analysis. Plasma samples were processed with methanol/acetonitrile, dried, re-dissolved, and centrifuged before

ultra-high-performance liquid chromatography–quadrupole time-of-flight (UHPLC-Q-TOF) analysis. Hydrophilic-interaction liquid chromatography (HILIC) separation used an ACQUITY UPLC BEH Amide column with a gradient of ammonium acetate/ammonium hydroxide in water and acetonitrile. Mass spectrometry/mass spectrometry (MS/MS) acquisition and data processing followed standard protocols, including Collection of Algorithms for MEtabolite pRofile Annotation (CAMERA) annotation and compound identification using an in-house database. Raw data were processed using XCMS for peak detection and alignment, and metabolites were annotated with CAMERA.

RNA-sequencing analysis

Total RNA was isolated from six lung samples each from the MCT and NTM groups. RNA quantity and integrity were evaluated using the K5500 (Beijing Kaiao, China) and the Agilent 2200 Tape Station (Agilent Technologies, USA). The mRNA enrichment was performed using oligo-dT according to the NEBNext® Poly(A) mRNA Magnetic Isolation Module (NEB, USA), followed by fragmentation to approximately 200 bp. The RNA fragments underwent first- and second-strand cDNA synthesis, adaptor ligation, and low-cycle enrichment using the NEBNext® Ultra™ RNA Library Prep Kit for Illumina. Purified library products were quality-checked using the Agilent 2200 Tape Station and Qubit (Thermo Fisher Scientific, USA). Sequencing was conducted using Illumina paired-end 150-bp sequencing at Ribobio Co. Ltd (Ribobio, China).

Raw data were cleaned by removing adaptor sequences, poly-N sequences, and low-quality reads. The clean reads were aligned to the rat reference genome mm10 using HISAT2 with default parameters. HTSeq was used to convert the aligned short reads into read counts for each gene model. Differential expression analysis was carried out using DESeq2, identifying differentially expressed genes (DEGs) based on a $|\log_2(\text{fold change})| > 1$ and a p value < 0.05. All of the identified DEGs underwent volcano plot and Kyoto Encyclopedia of Genes and Genomes (KEGG) ontology enrichment analyses with significance determined at $p < 0.05$.

RNA extraction and quantitative Polymerase Chain Reaction (qPCR)

Lung tissues from the MCT and NTM group were collected and immediately frozen in liquid nitrogen. Total RNA was extracted using TRIzol reagent (Invitrogen, Cat# 15596018), followed by chloroform extraction. After quantifying the concentrations and purities of RNA, GoScript™ Reverse Transcriptase (Promega, Cat# A5000) was used for RNA reverse transcription in accordance with the manufacturer's protocols. Subsequently, cDNA from the samples was amplified, and the expression levels were determined with SYBR Green qPCR Master Mix (EZBioscience, Cat# A0001) on the Roche LightCycler 480 System. The transcript expression levels of each gene were standardized to that of endogenous control gene β-actin and expressed as a relative ratio to the mean values of control samples. The primer sequences are listed in Table S1.

Statistical analysis

The two-tailed Student's *t* test was used to compare haemodynamic parameters between two groups, while One-way Analysis of Variance (ANOVA) assessed differences among three groups. The $\chi 2$ test was utilized to compare gender. The Fisher's exact test was utilized to compare diet. The Mann–Whitney *U* test was used to compare microbial community indicators between two groups, and the Kruskal–Wallis test determined significant differences among three groups. Rarefaction curves assessed sequencing depth for each sample. Alpha diversity of GM was assessed using the Chao1 and Shannon indexes. PCoA analysed beta diversity based on Bray–Curtis distance, considering the relative abundance of archaeal, fungal, and bacterial species using the vegan R package. Adonis analysis based on Bray–Curtis dissimilarity tested differences in microbial composition between groups. Pulmonary vascular muscularization and media thickness percentages were compared using one-way ANOVA. Spearman correlation analysis was performed on differential microbial communities and haemodynamic parameters in IPAH patients and rat models. Areas under the Receiver operating characteristic (ROC) curves (AUCs) were determined using multiple logistic regression. Statistical analyses were conducted using R (v4.2.2) and GraphPad Prism (version 9.0). p values lower than 0.05 were considered statistically significant, and numerical data were presented as mean ± standard deviation (S.D.).

Role of the funding source

Funders did not have any role in the study design, data collection, data analyses, interpretation, or writing of the study.

Results

Gut bacterial, archaeal, and fungal microbiota are altered in IPAH patients

Fecal samples were collected from 31 HCs to 31 IPAH patients. Basic clinical metadata are presented in Table 1. There were no significant differences in mean age ($p = 0.164$) and mean body mass index (BMI) ($p = 0.174$) between the HC and IPAH groups. Additionally, the distribution of sex was equally balanced between the HC and IPAH groups ($p = 0.446$) and the distribution of diet patterns was not significantly different between the two groups ($p = 1.000$), indicating that these demographic variables were well-matched. IPAH patients exhibited a mean pulmonary arterial

	CON (n = 31)	IPAH (n = 31)	p value
Age (SD)	34.5 ± 11.9	39.1 ± 13.6	0.163
Male (%)	17 (54.8)	14 (45.2)	0.446
BMI	23 ± 2.4	23.9 ± 3	0.174
NYHA I/II/III/IV(n)	NA	3/10/17/1	NA
Cardiac index (L/min/m^2)	NA	2.6 ± 0.5	NA
Cardiac output (L/min)	NA	4.1 (1)	NA
Pulmonary vascular resistance (WU)	NA	9.3 ± 2.9	NA
Pulmonary artery wedge pressure (mmHg)	NA	10.5 ± 4.7	NA
Mean pulmonary artery pressure (mmHg)	NA	46.8 ± 9.4	NA
Right ventricular systolic pressure (mmHg)	NA	72.3 ± 14.9	NA
Mean right atrial pressure (mmHg)	NA	9.5 ± 3.7	NA
NT-proBNP (pg/mL)	NA	2467.5 ± 3276.5	NA
6MWD (m)	NA	363.3 ± 97.6	NA
TAPSE (mm)	NA	7.9 ± 7	NA
Diet,n (%)			>0.999
Omnivore	29 (93.5)	28 (90.3)	>0.999
Pescatarian	0	1 (3.2)	>0.999
Vegetarian	1 (3.2)	2 (6.4)	>0.999
Vegan	0	0	>0.999
Other	1 (3.2)	0	>0.999

Data following a normal distribution are presented as mean ± standard deviation; Gender was shown as percentage (%). The analysis of age and BMI was conducted using Two-tailed Student's t-test. The χ 2 test was utilized to compare gender. The Fisher's exact test was utilized to compare diet. NA, indicates not applicable; BMI, Body Mass Index; 6MWD, six minutes-walk distance; TAPSE, tricuspid annular plane systolic excursion; NT-proBNP, N-terminal pro-B-type natriuretic peptide; NYHA, New York Heart Association.

Table 1: **Baseline demographics and clinical characteristics of the study participants.**

pressure (mPAP) of 46.8 ± 9.4 mm Hg, a mean RVSP of 72.3 ± 14.9 mm Hg, a mean 6-min walk distance (6MWD) of 363.3 ± 97.6 m, and a cardiac output of 2.6 ± 0.5 L/min/m^2.

The shotgun metagenomics was used to analyse the alterations in the multi-kingdom gut microbial community, including bacteria, fungi, and archaea, in IPAH patients. As shown in Table S2, after quality-filtering, the total number of clean reads was 4,487,697,472, with an average of 72,382,217 reads per sample. Based on the clean reads, we detected the numbers of bacteria, archaea, and fungi at each taxonomic level, as presented in Table S3.

We further characterized the community structural changes of bacteria, archaea, and fungi at the species level using alpha diversity and beta diversity indexes. PCoA based on Bray–Curtis dissimilarity indicated significant differences in the gut taxonomic composition among bacterial, archaeal, and fungal communities between the two groups (Bacteria: Adonis, $R^2 = 0.05$, $p = 0.001$; Archaea: Adonis, $R^2 = 0.03$, $p = 0.049$; Fungi: Adonis, $R^2 = 0.04$, $p = 0.045$; Fig. 1a–c). Compared with the HC group, only the richness index Chao1 was higher in the IPAH group for fungi (Fig. 1d–i).

Additionally, we analysed the taxonomic abundance of bacteria, fungi, and archaea at the species level. Within the bacterial community, the top-five species identified were *Faecalibacterium prausnitzii*, *Blautia wexlerae*, *Eubacterium rectale*, *Bacteroides uniformis*, and *Escherichia coli* (Fig. 1j). Within the archaeal community, *Methanobrevibacter smithii*, *Nitrosopumilus SGB14899*, *Methanobrevibacter oralis*, *Methanolacinia petrolearia*, and *Methanomethylovorans SGB40959* emerged as the top-five species (Fig. 1k). In the fungal community, the top-five species were *Schizosaccharomyces pombe*, *Fusarium pseudograminearum*, *Thermothielavioides terrestris*, *Colletotrichum higginsianum*, and *Lachancea kluyveri* (Fig. 1l). The LEfSe analysis revealed distinct microbial signatures between the HC and IPAH groups (Figure S1). These data suggest that IPAH patients have a distinct structure and composition of GM, including bacteria, archaea, and fungi, compared with HCs.

Fecal microbiota transplantation from IPAH patients induces phenotypic changes of PAH in rats

To further explore the relationship between GM dysbiosis and PAH, we used two different FMT models, namely the IPAH patient-to-rat FMT model (Fig. 2a) and the PAH rat-to-rat FMT model (Fig. 3a). Before FMT, antibiotics were administered for four consecutive days to deplete the original GM from the recipient SD rats, thereby facilitating the colonization of newly introduced microorganisms. Fecal microbiota from the HC donors and IPAH patient donors were transplanted into the recipient rats (the HTN and PTN groups, respectively) daily by gavage for 2 weeks. After 8 weeks, there was no significant difference in the RV hypertrophy index (RVHI) between the two groups of rats, but the PTN rats

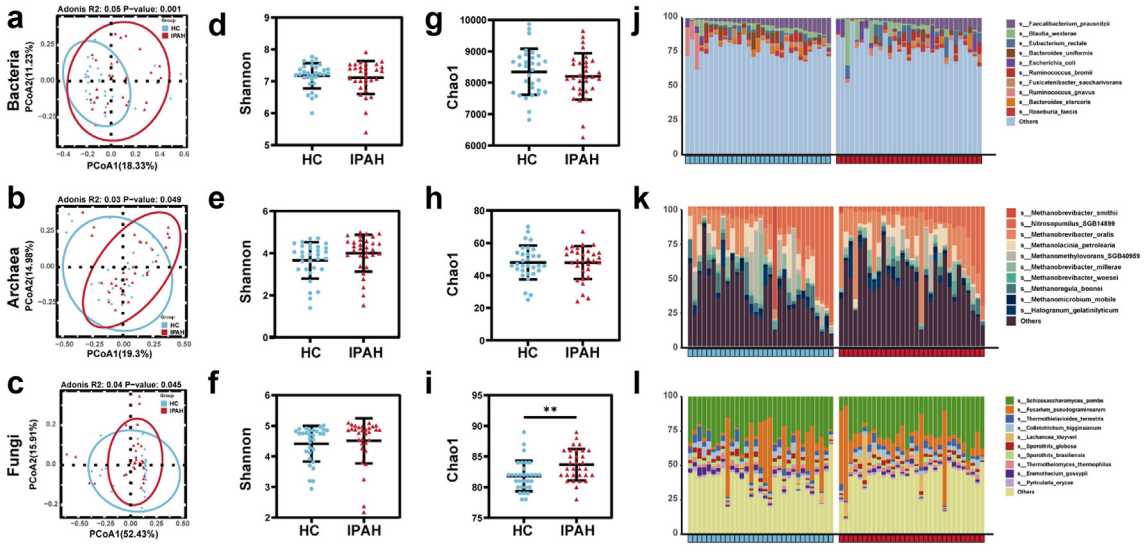

Fig. 1: **Gut bacterial, archaeal, and fungal microbiota are altered in idiopathic pulmonary arterial hypertension (IPAH) patients.** (**a**) Principal coordinate analysis (PCoA) diagram of bacterial communities based on Bray–Curtis dissimilarity between the healthy control (HC) and IPAH groups. (**b**) PCoA diagram of archaeal communities based on Bray–Curtis dissimilarity between the HC and IPAH groups. (**c**) PCoA diagram of fungal communities based on Bray–Curtis dissimilarity between the HC and IPAH groups. Dissimilarity was assessed using the Adonis method. (**d–f**) Shannon indexes of bacterial (**d**), archaeal (**e**), and fungal (**f**) communities at the species level between healthy controls and patients with IPAH. (**g–i**) Chao1 indexes of bacterial (**g**), archaeal (**h**), and fungal (**i**) communities at the species level between healthy controls and patients with IPAH. (**j**) Relative abundance of bacterial species between the HC and IPAH groups. (**k**) Relative abundance of archaeal species between the HC and IPAH groups. (**l**) Relative abundance of fungal species between the HC and IPAH groups. n = 31. **p < 0.01 indicates significant differences. (d–i) by two-tailed Student's *t* test.

showed a significant increase in RVSP (Fig. 2b and c), indicating elevated pulmonary arterial pressure. Echocardiography revealed significantly decreased PAAT and TAPSE, indicating increased pulmonary vascular resistance. Additionally, increased RVWT and RVEDD indicated altered RV morphology and function (Fig. 2d and e).

Consistent with the observed haemodynamic changes, the PTN rats exhibited increased pulmonary vascular wall thickness and muscularization, as revealed by HE and EVG staining (Fig. 2f). In the HTN group, the predominant vessels of this calibre typically exhibited an NPA phenotype. In contrast, in the PTN group, there was a significant decrease in the prevalence of NPA vessels, which was accompanied by a marked increase in the prevalence of PPA vessels (Fig. 2g). Furthermore, the media wall thickness of pulmonary arteries with diameters less than 50 μm significantly increased in the PTN group (Fig. 2h).

Fecal microbiota transplantation from MCT-PAH rats induces phenotypic changes of pulmonary arterial hypertension in rats

We next transplanted the fecal microbiota from the normal control rats and MCT-induced PAH rats into the recipient rats (the NTN and MTN groups, respectively) by gavage for 2 weeks (Fig. 3a). To validate the efficacy of the ABX protocol and FMT, metagenomics analysis was performed on the fecal samples from the respective groups of rats. The findings demonstrated that the ABX protocol significantly reduced alpha diversity of the microbial communities, indicating successful depletion of the indigenous GM (Figure S2). Furthermore, FMT effectively transferred the donor's microbial community structure to the recipient rats, as evidenced by the establishment of a microbiota profile that closely resembled that of the donor rats (Figure S3). Eight weeks following FMT, the MTN rats exhibited a significant increase in RVSP compared with the NTN rats (Fig. 3b). However, there was no significant difference in RVHI between the NTN and MTN groups (Fig. 3c). PAAT, RVWT, TAPSE, and RVEDD were all significantly worsened in the MTN group (Fig. 3d and e). Correspondingly, FMT exacerbated lung vascular remodelling, as revealed by HE and EVG staining (Fig. 3f).

Comparison of the pulmonary arterioles between the two groups of rats revealed that the musculature levels of the three types of vessels—NPA, PPA, and MPA—were largely similar across the two groups (Fig. 3g). However, pulmonary arteries with diameters less than 50 μm exhibited increased media wall thickness (Fig. 3h). Taken together, these results indicate that the GM modulates pulmonary vascular remodelling in response to FMT.

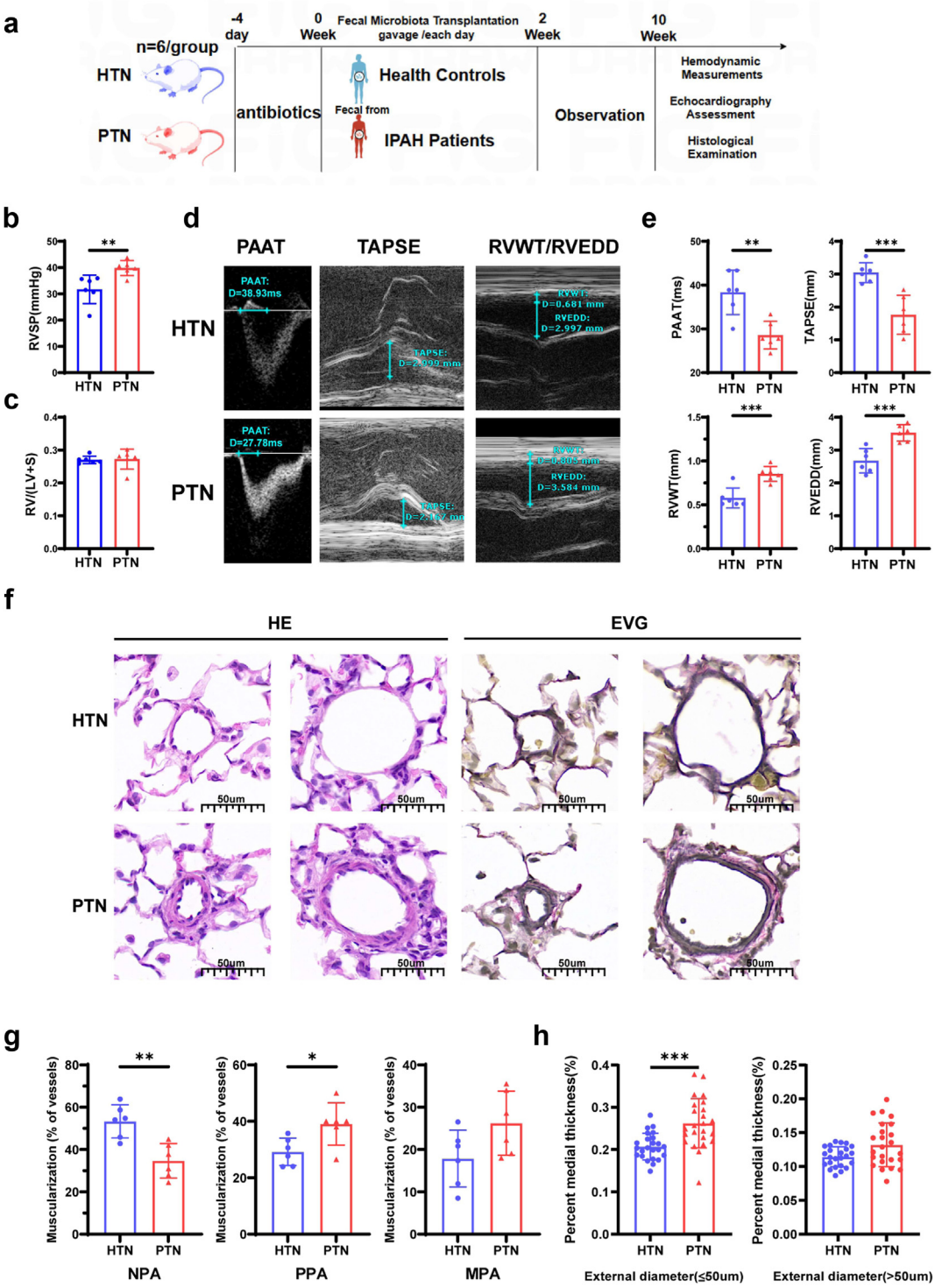

Fig. 2: **Fecal microbiota transplantation (FMT) from IPAH patients induces phenotypes of PAH and pulmonary vascular remodelling in rats**. (**a**) Schematic overview and timeline of the IPAH patient-to-rat FMT model. (**b** and **c**) Bar graphs showing RVSP and RVHI (RV/LV + S) in HTN and PTN rats (n = 6 rats per group). (**d**) Representative echocardiographic images of HTN and PTN rats for PAAT, TAPSE, RVWT, and RVEDD. (**e**) Echocardiography measurements of PAAT, TAPSE, RVWT, and RVEDD in HTN and PTN rats (n = 6 rats per group). (**f**) Representative photomicrographs of lung sections from HTN and PTN rats stained with haematoxylin and eosin (HE) and Elastic-van Gieson (EVG) staining. Scale bars: 50 μm. (**g**) Proportion of nonmuscularized (NPA), partially muscularized (PPA), and fully muscularized (MPA) pulmonary arterioles

Remission of pulmonary arterial pressure and vasculature remodelling in PAH rats through fecal microbiota transplantation therapy

To comprehensively explore the influence of FMT on PAH, we established a therapeutic FMT model simulating the clinical scenario when the disease is diagnosed in humans. Given the antibiotic treatment effects in hypoxia-induced PAH,[18] we developed a fecal transplantation model without antibiotics to test whether specific gut flora can attenuate PAH progression. In this protocol, the GM from normal controls (CON group) was transplanted into the MCT-induced PAH rats (NTM group) for 3 weeks following intraperitoneal injection with 60 mg/kg body weight MCT. Concurrently, the MCT rats were intraperitoneally injected with MCT and received placebo gavage for 3 weeks (MCT group). All rats were sacrificed on day 28 (Fig. 4a).

The results showed that FMT significantly improved the PAH phenotype in the MCT-PAH rats (Fig. 4b–h). Compared with the CON group, the MCT rats exhibited a significant increase in RVSP and a decrease in PAAT, indicating increased pulmonary vascular resistance (Fig. 4b–e). Alterations in RV function and morphology were determined by higher RVHI, RVEDD, and RVWT, along with shortened TAPSE in the MCT group (Fig. 4c–e). However, FMT therapy reversed these phenotypes in the NTM group (Fig. 4b–e).

To further investigate the effects of FMT on the PAH phenotype, we conducted the same experimental protocol in female rats. Specifically, we transplanted the GM from healthy female rats (CON-F group) into the MCT-induced PAH female rats (NTM-F group). The results showed that FMT significantly alleviated RVSP and RVWT (Figure S4a, d) in the NTM-F group. Furthermore, compared with the MCT-F group, the NTM-F group showed a decreasing trend in RVHI and RVEDD, while PAAT and TAPSE showed an increasing trend (Figure S4b, d). These results suggest that, similar to the findings in male rats, FMT alleviated the severity of PAH in female rats. In line with the observed haemodynamic changes, FMT alleviated pulmonary vessel remodelling in the MCT rats (Fig. 4f). Although FMT therapy did not affect the muscularization ratio of pulmonary vessels, it significantly reversed pulmonary microvasculature remodelling, especially in pulmonary vessels with diameters less than 50 μm (Fig. 4g and h).

These results suggest that, in contrast to the GM from the IPAH model, which promotes PAH progression, the GM from normal control rats contributes to PAH recovery by attenuating pulmonary vasculature remodelling.

Fecal microbiota transplantation therapy ameliorates gut bacterial, archaeal, and fungal microbiota dysbiosis in PAH rats

To ascertain the mechanisms underlying the GM recovery in PAH, shotgun metagenomics was performed in the CON, MCT, and NTM rats. As shown in Table S4, the total number of sequences was 785,394,069, with an average of 43,633,004 reads per sample. Based on the clean reads, the numbers of bacteria, archaea, and fungi at each taxonomic level are shown in Table S5. We characterized the ecological features using alpha and beta diversity indexes at the species level. PCoA based on Bray–Curtis dissimilarity demonstrated significant differences in the structure and composition of the GM among CON, MCT, and NTM groups. (Adonis: Bacteria: $R^2 = 0.32$, $p = 0.002$; Archaea: $R^2 = 0.21$, $p = 0.009$; Fungi: $R^2 = 0.19$, $p = 0.096$; Fig. 5a–c). In contrast, the GM structure and composition, including bacteria, archaea, and fungi, of the NTM group resembled that of the CON group, suggesting successful colonization of the recipient rat gut by the donor microbiota following FMT (Figure S5). Alpha diversity analysis based on Chao1 and Shannon indexes showed no significant differences among the CON, MCT, and NTM groups for bacteria, fungi, and archaea (Figure S6). We hypothesized that the success of FMT therapy might have arisen from establishing beneficial microbial communities and eliminating pathogenic agents contributing to PAH. To elucidate the therapeutic mechanisms of FMT, we conducted LEfSe analysis to investigate differential microbial communities among the CON, MCT, and NTM groups at the levels of bacteria, archaea, and fungi (Figure S7, LDA score >2). To comprehensively understand the role of microbial communities in PAH, we employed a heat map visualization to depict the significantly differential microbial taxa identified through the LEfSe analysis. We focused on the taxa exhibiting abundance alterations in the MCT group that were reversed in the NTM group at the species level, shedding light on their potential mechanisms of action (Fig. 5d).

We identified 78 distinct bacterial species within the microbial community, with 49 species enriched in the CON and NTM groups and 29 species enriched in the MCT group. Concerning archaeal communities, out of four distinct archaeal species, two species were enriched in the CON and NTM groups, while two species were enriched in the MCT group. Similarly, in the fungal community, five distinct fungal species were identified, with three enriched in the CON and NTM groups and two enriched in the MCT group.

(<100 μm in diameter) in HTN and PTN rats (n = 6 rats per group). (**h**) Quantification of vascular media thickness from images in (E) (n = 6 rats per group, four PAs per rat). HTN, healthy to normal group; PTN, IPAH to normal group; RVSP, right ventricular systolic pressure; RVHI, right ventricular hypertrophy index; PAAT, pulmonary arterial acceleration time; TAPSE, tricuspid annular plane systolic excursion; RVEDD, right ventricular end-diastolic dimension; RVWT, right ventricular free wall thickness. Results are expressed as mean ± SD. *p < 0.05, **p < 0.01, ***p < 0.001, (b, c, e, g, h) by two-tailed Student's *t* test.

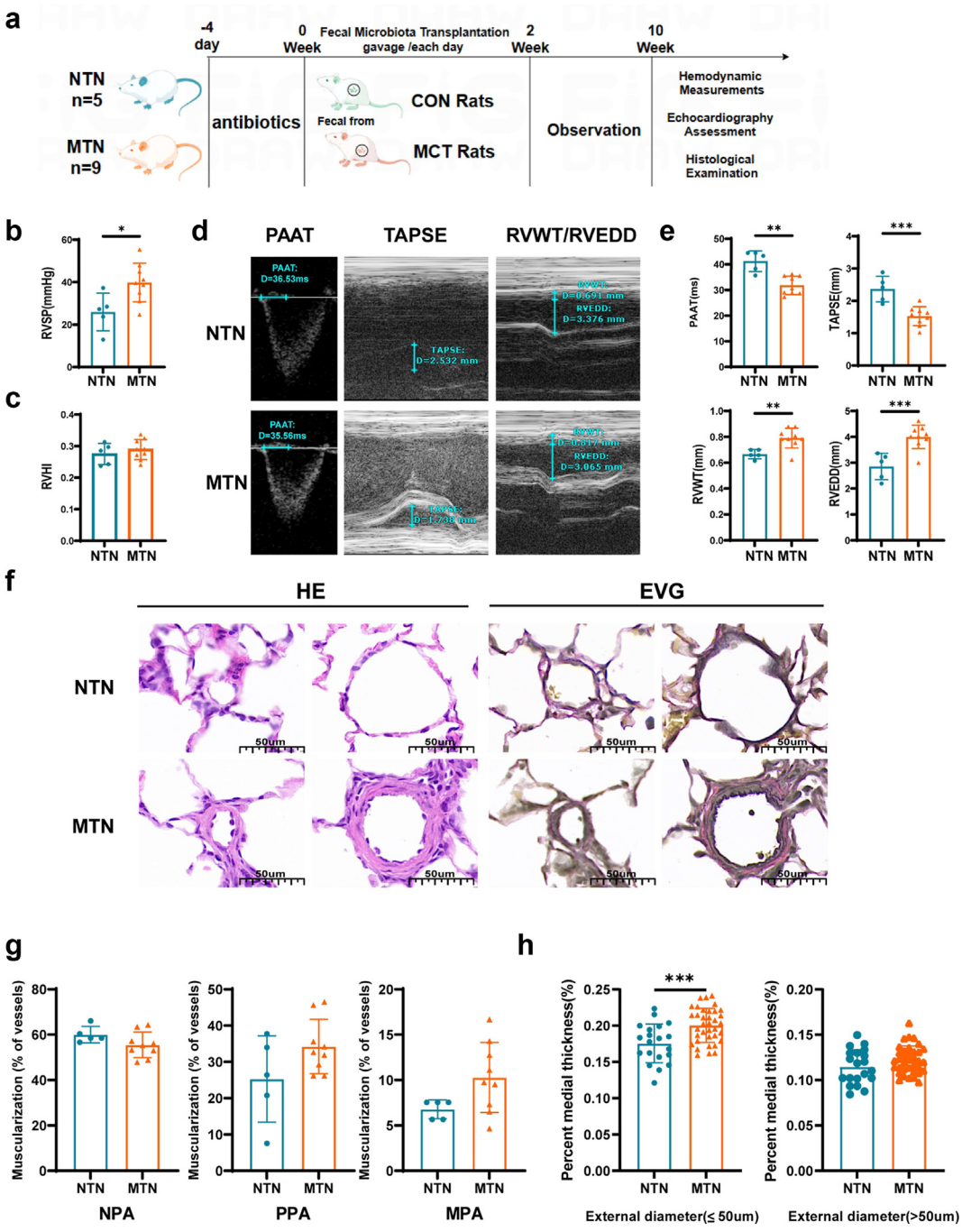

***Fig. 3:* FMT from MCT-PAH rats induces phenotypes of PAH and pulmonary vascular remodelling in rats**. (**a**) Schematic overview and timeline of the MCT-PAH rat-to-rat FMT model. (**b** and **c**) Bar graphs showing RVSP and RVHI (RV/LV + S) in NTN and MTN rats (n = 5 for the NTN group; n = 9 for the MTN group). (**d**) Representative echocardiographic images of NTN and MTN rats for PAAT, TAPSE, RVWT, and RVEDD. (**e**) Echocardiography measurements of PAAT, TAPSE, RVWT, and RVEDD in NTN and MTN rats (n = 5 for the NTN group; n = 9 for the MTN group). (**f**) Representative photomicrographs of lung sections from NTN and MTN rats stained with haematoxylin and eosin (HE) and Elastic-van Gieson (EVG) staining. Scale bars: 50 μm. (**g**) Proportion of nonmuscularized (NPA), partially muscularized (PPA), and fully muscularized (MPA) pulmonary arterioles (<100 μm in diameter) in NTN and MTN rats (n = 5 for NTN group; n = 9 for MTN group). (**h**) Quantification of vascular medial thickness from images in (**e**) (n = 5 for NTN group; n = 9 for MTN group, four PAs per rat). NTN, normal to normal group; MTN, MCT-PAH to normal group; RVSP, right ventricular systolic pressure; RVHI, right ventricular hypertrophy index; PAAT, pulmonary arterial acceleration time; TAPSE, tricuspid annular plane systolic excursion; RVEDD, right ventricular end-diastolic dimension; RVWT, right ventricular free wall thickness. Results are expressed as mean ± SD. *p < 0.05, **p < 0.01; (b, c, e, g, h) by two-tailed Student's *t* test.

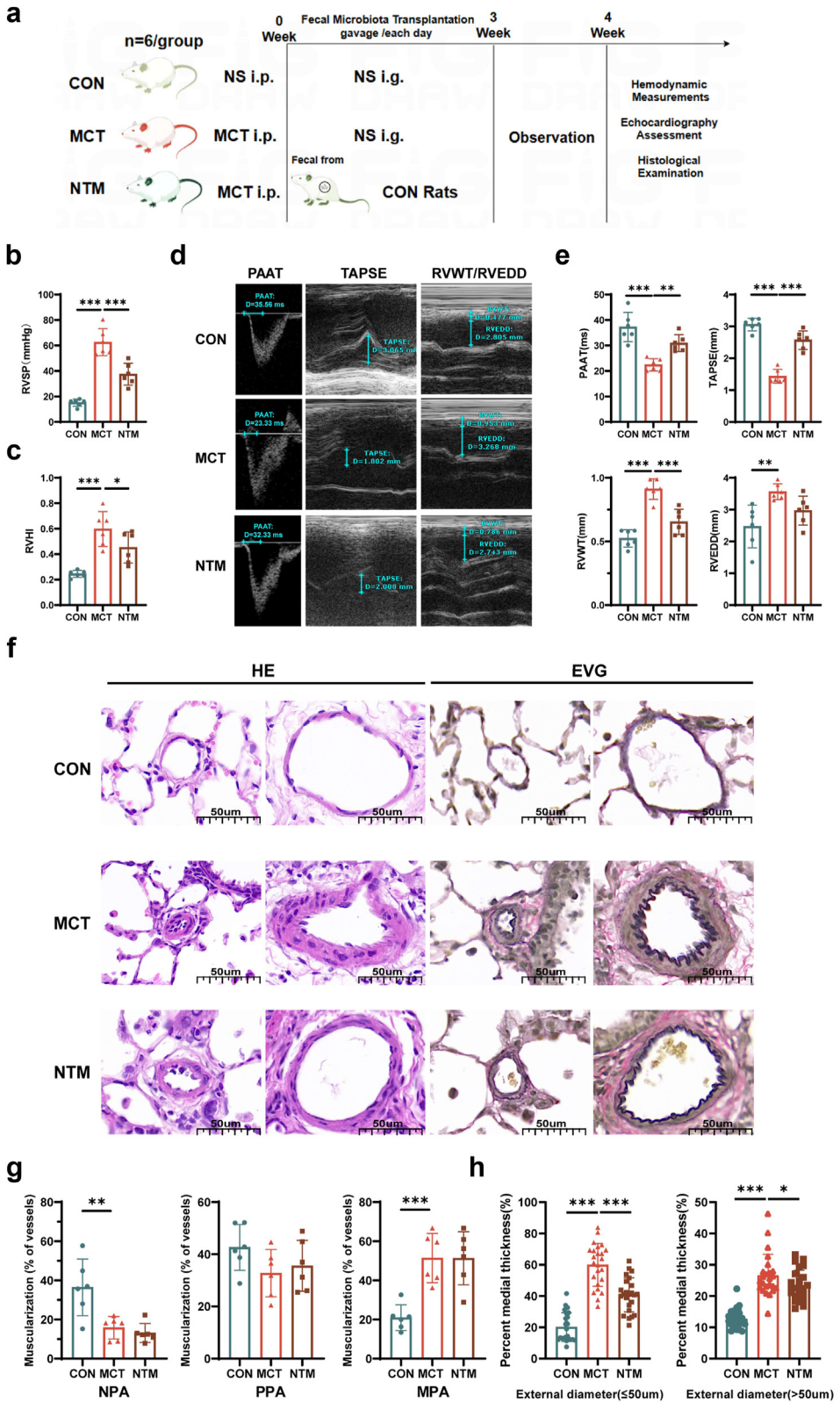
a
n=6/group
0 Week
Fecal Microbiota Transplantation gavage /each day
3 Week
4 Week
CON
NS i.p.
NS i.g.
MCT
MCT i.p.
NS i.g.
NTM
MCT i.p.
Fecal from
CON Rats
Observation
Hemodynamic Measurements
Echocardiography Assessment
Histological Examination
b
RVSP (mmHg)
c
RVHI
d
PAAT
TAPSE
RVWT/RVEDD
CON
MCT
NTM
e
PAAT(ms)
TAPSE(mm)
RVWT(mm)
RVEDD(mm)
f
HE
EVG
CON
MCT
NTM
50um
g
Muscularization (% of vessels)
NPA
PPA
MPA
h
Percent medial thickness(%)
External diameter(≤50um)
External diameter(>50um)

Furthermore, Spearman correlation analysis revealed strong correlations between various haemodynamic and RV ultrasound indexes—such as RVSP, RVHI, PAAT, RVWT, and RVEED—and GM characteristics, including bacteria, archaea, and fungi (Fig. 5e). These findings underscore the considerable alterations in both the composition and functionality of the GM in PAH.

Fecal microbiota transplantation alters serum metabolite composition in rats

Since the GM often influences disease progression by metabolizing substances that act on target organs,[19] we conducted untargeted metabolomics analysis on serum samples from each group of rats. Principal component analysis (PCA) revealed distinct separation of metabolic profiles among the CON, MCT, and NTM groups (Fig. 6a). Bar graphs shown in Fig. 6b depict lipids and lipid-like molecules, organic acids and derivatives, phenylpropanoids, and polyketides as the major metabolites in serum. Volcano plots shown in Fig. 6c and d further illustrate the absolute abundances of metabolites in serum between the CON and MCT groups and between the MCT and NTM groups. Specifically, based on the criteria of $|\log2\text{fold-change}| \geq 0.58$ and $p < 0.05$, our analysis identified 153 upregulated and 61 downregulated metabolites between the CON and MCT groups. Similarly, there were 128 upregulated and 47 downregulated metabolites between the MCT and NTM groups. Based on the results of differential analysis, we selected the metabolites that changed in PAH and were reversed by FMT, visualizing these changes in a heat map format (Fig. 6e).

To further investigate the interplay among the GM, serum metabolites, and PAH, we conducted Spearman correlation analyses between differential GM, serum differential metabolites, and haemodynamic parameters. We visualized these correlation analyses using a Sankey diagram (Figure S8). Our findings revealed close correlations between the GM, metabolites, and PAH-related indexes. Alpha-ketoisovaleric acid emerged as the metabolite with the strongest correlation with PAH indexes among the serum metabolites. In summary, our data provide evidence supporting the influence of the GM on the occurrence and progression of PAH through modulation of serum metabolites.

Fecal microbiota transplantation modifies the core signalling pathways involved in PAH

To explore the mechanisms by which FMT alleviates PAH, we conducted RNA-sequencing analysis on lung tissues isolated from the MCT and NTM rats (Fig. 7). DEGs were identified using a threshold of $|\log2\text{fold change}| \geq 1$ and $p \leq 0.05$. The analysis revealed that 737 genes were differentially expressed in the NTM rats compared with the MCT rats, with 394 upregulated and 340 downregulated genes (Fig. 7a). To substantiate the transcriptomic findings, we performed qPCR validation on six randomly selected DEGs, as shown in Figure S9. These genes included cluster of differentiation 19 (CD19), phospholipase A2 group IIa (PLA2G2a), leucocyte immunoglobulin-like receptor subfamily B member 1b (LILRB1b), tumour necrosis factor receptor superfamily member 13c (TNFRSF13c), calcium channel voltage-dependent L type alpha 1f (CACNA1f), and calmodulin-like 5 (CALML5). The qPCR results corroborated the differential expression patterns observed in the RNA-sequencing data, further validating the regulatory impact of FMT on these genes in the context of PAH.

To further understand the signalling pathways associated with these DEGs in the NTM group, KEGG pathway enrichment analysis was performed. Through FMT treatment, the enriched KEGG pathways were found to be associated with vascular inflammation and vascular remodelling, which are fundamental pathological mechanisms of PAH. These pathways included leucocyte transendothelial migration, cytokine–cytokine receptor interaction, and cell adhesion molecules (Fig. 7b). Additionally, pathways related to vascular smooth muscle contraction were also significantly enriched. These findings indicate that FMT therapy could mitigate PAH progression by reducing vascular inflammation and vascular remodelling and easing pulmonary vasoconstriction.

Diagnostic potential of differentially enriched microbiota in idiopathic pulmonary arterial hypertension

Subsequently, we identified seven microbial species, including three bacterial species, one archaeon, and three fungal species, which exhibited the overlapping

Fig. 4: **Reversal of pulmonary arterial pressure and vasculature remodelling in PAH rats through FMT therapy.** (**a**) Schematic overview and timeline of the FMT therapy model. (**b** and **c**) Bar graphs showing RVSP (mm Hg) and RVHI (RV/LV + S) in CON, MCT, and NTM rats. (**d**) Echocardiographic measurements and images of PAAT, TAPSE, RVWT, and RVEDD in CON, MCT, and NTM rats. (**e**) Echocardiography measurements of PAAT, TAPSE, RVWT, and RVEDD in CON, MCT, and NTM rats. (**f**) Representative photomicrographs of lung sections from CON, MCT, and NTM rats stained with haematoxylin and eosin (HE) and Elastic-van Gieson (EVG) staining. Scale bars: 50 μm. (**g**) Proportion of nonmuscularized (NPA), partially muscularized (PPA), and fully muscularized (MPA) pulmonary arterioles (<100 μm in diameter) in CON, MCT, and NTM rats. (**h**) Quantification of vascular media thickness from images in (**f**) (n = 6 rats per group, four PAs per rat). CON, normal group; MCT, MCT-PAH group; NTM, normal to MCT-PAH group; RVSP, right ventricular systolic pressure; RVHI, right ventricular hypertrophy index; PAAT, pulmonary arterial acceleration time; TAPSE, tricuspid annular plane systolic excursion; RVEDD, right ventricular end-diastolic dimension; RVWT, right ventricular free wall thickness. Results are expressed as mean ± S.D. *p < 0.05, **p < 0.01, ***p < 0.001. NS: normal saline; i.p.: intraperitoneal injection; i.g.: gavage. (b, c, e, g, h) by one-way ANOVA; Holm–Sidak's multiple-comparisons test.

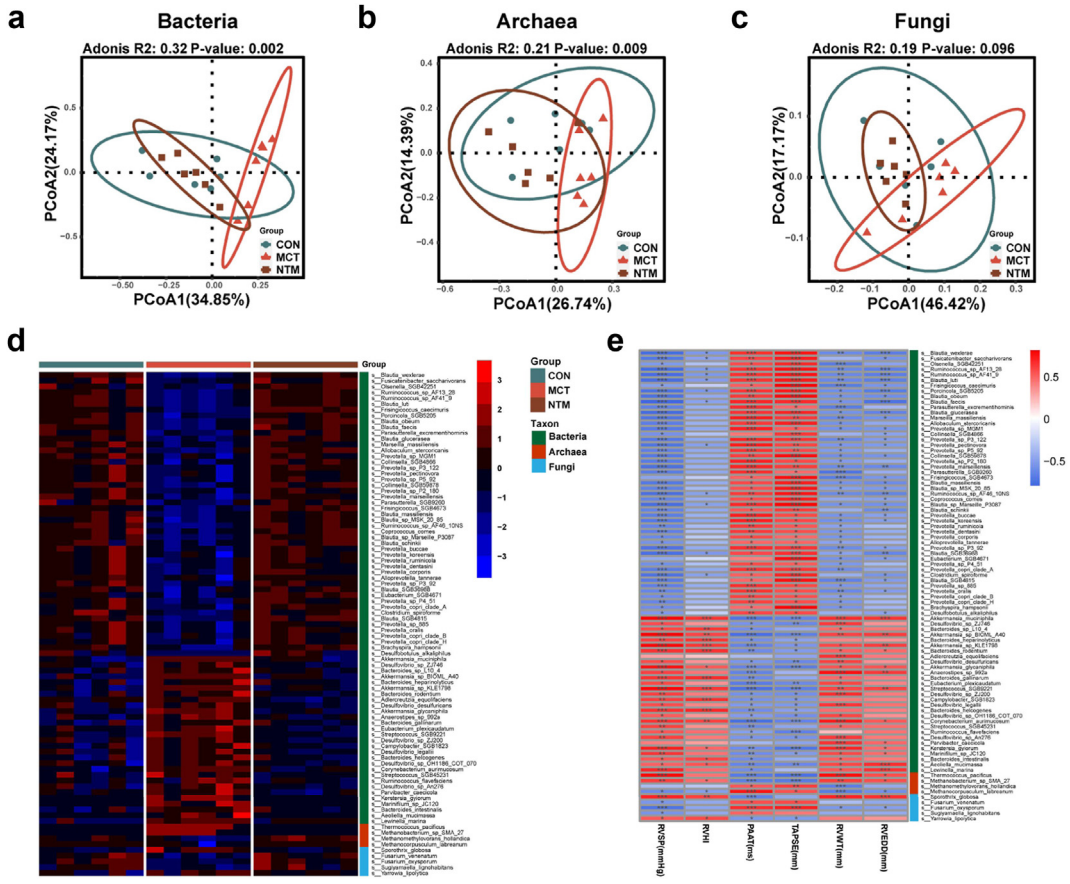

Fig. 5: **FMT restores dysbiosis of gut microbiota in MCT-PAH rats**. (**a**) Principal coordinate analysis (PCoA) diagram of bacterial communities based on Bray–Curtis dissimilarity among CON, MCT, and NTM groups (n = 6). (**b**) PCoA diagram of archaeal communities based on Bray–Curtis dissimilarity among CON, MCT, and NTM groups (n = 6). (**c**) PCoA diagram of fungal communities based on Bray–Curtis dissimilarity among CON, MCT, and NTM groups (n = 6). Dissimilarity was assessed using the Adonis method. (**d**) Heat map showing clustering of bacterial, archaeal, and fungal communities with their relative abundances at the species level. (**e**) Heat map of Spearman's correlation coefficients between different microbiota and haemodynamic parameters from all samples in the three groups (n = 6 per group). The gradient colours represent the correlation coefficients, with red indicating positive correlations and blue indicating negative correlations. *p < 0.05, **p < 0.01, ***p < 0.001.

differential abundance trends in rats (CON and MCT groups) and humans (HC and IPAH cohorts). We visualized the relative abundance of these differential kingdom microbiota using a heat map (Fig. 8a). We next explored the performance of the single-kingdom markers and the combined multi-kingdom markers by ROC analysis to investigate the diagnostic utility of these differentially enriched microbiota for IPAH (Fig. 8b). Surprisingly, we discovered that the diagnostic performance of any two kingdom combinations was superior to that of individual communities, with the highest diagnostic efficacy observed when all three kingdoms were combined, achieving an AUC of 0.881. Given the excellent diagnostic performance of the GMs, we further explored their correlation with haemodynamic parameters. Our results indicated that *Blautia obeum* negatively correlated with patients' PVR and RVSP (Fig. 8c and d). These findings provide further validation of the observations from animal studies.

Discussion

This study investigated the role of multi-kingdom GM, including bacteria, fungi, and archaea, in PAH. We found significant alterations in the gut microbial communities in IPAH patients, indicated by changes in alpha and beta diversity indexes and specific microbial species. FMT from IPAH patients or MCT-induced PAH rats induced PAH phenotypes in recipient rats. Conversely, FMT from healthy rats ameliorated PAH, restoring GM composition and reversing PAH-associated serum metabolite changes. Additionally, strong correlations were found among the GM, metabolites, and PAH-related indexes. Finally, models

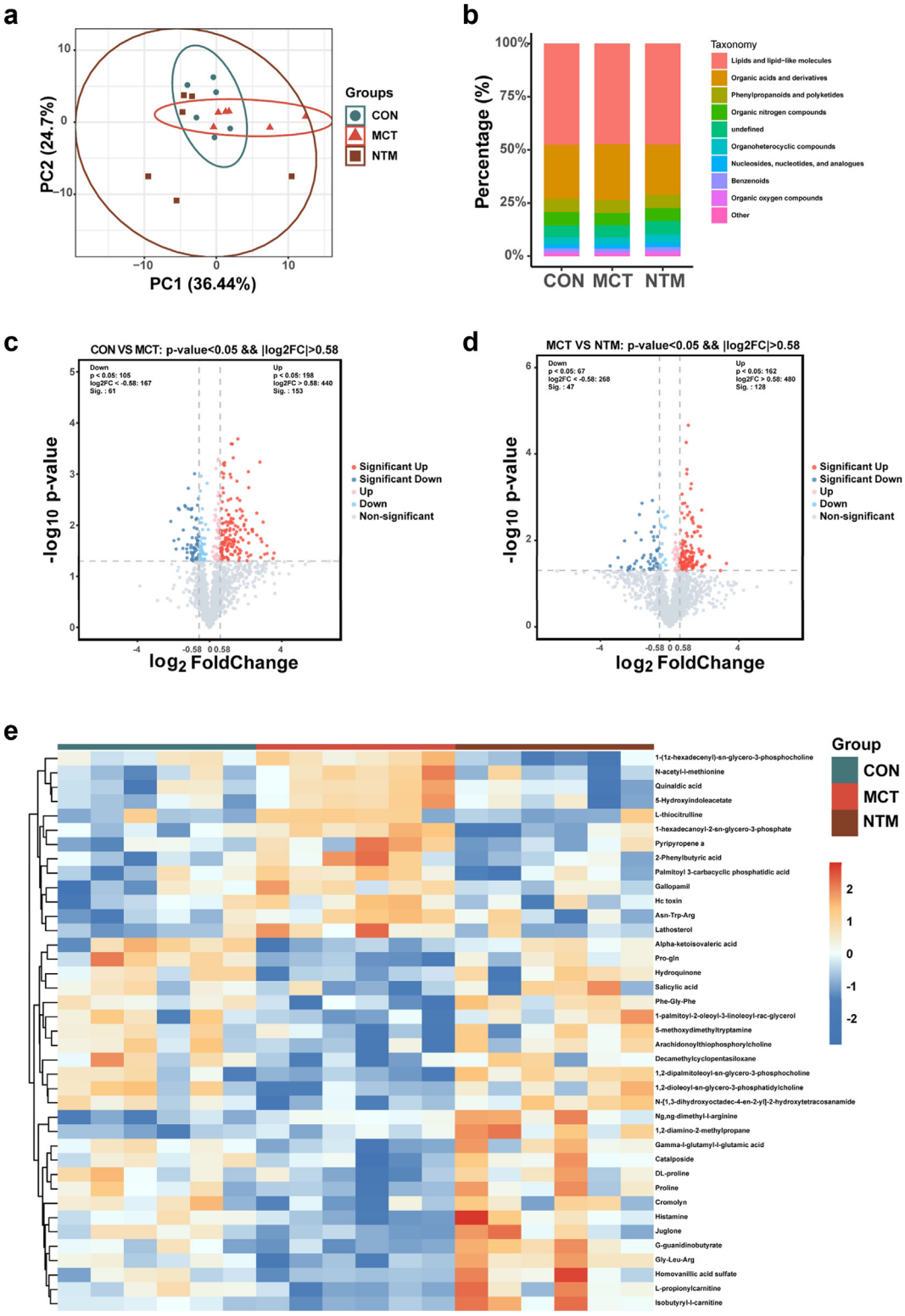

Fig. 6: **FMT alters serum metabolite composition in rats.** (**a**) PCA score plot for plasma metabolites. (**b**) Stacked bar graph of metabolite abundance. (**c**) Volcano plot of differentially expressed serum metabolites between the CON and MCT groups. (**d**) Volcano plot of differentially expressed serum metabolites between the MCT and NTM groups. (**e**) Community heat map of the differential metabolites that changed in the PAH group and were reversed by FMT.

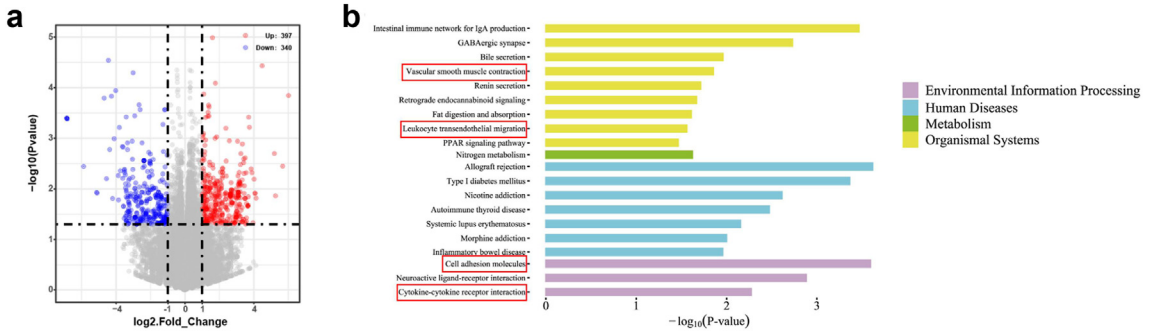

***Fig. 7:* Lung transcriptome changes in response to FMT treatment**. (**a**) Volcano plot of differentially expressed genes (DEGs) comparing the normal to MCT-PAH (NTM) group with the monocrotaline (MCT) group. Genes with |log2(FC)| > 1, indicating significant upregulation (right) or downregulation (left), are highlighted. The plot emphasizes the statistical significance of gene expression changes, with the y-axis representing the −log10 of the p value. (**b**) Enriched KEGG pathways in DEGs. The top pathways are shown, ranked by enrichment score, which quantifies the overrepresentation of DEGs within each pathway. This analysis reveals the biological processes most affected by the gene expression changes between the NTM and MCT groups.

using multi-kingdom markers from bacterial, archaeal, and fungal communities exhibited superior diagnostic performance. These findings underscore the critical role of the entire GM in PAH and highlight the therapeutic and diagnostic potential of microbiota-based interventions.

Previous studies have reported GM dysbiosis in PAH patients, characterized by reduced bacterial diversity and increased proinflammatory taxa.[9,12] Our study corroborates these findings, showing significant changes of bacterial community in both alpha and beta diversity indexes, indicating a disruption in the gut bacterial

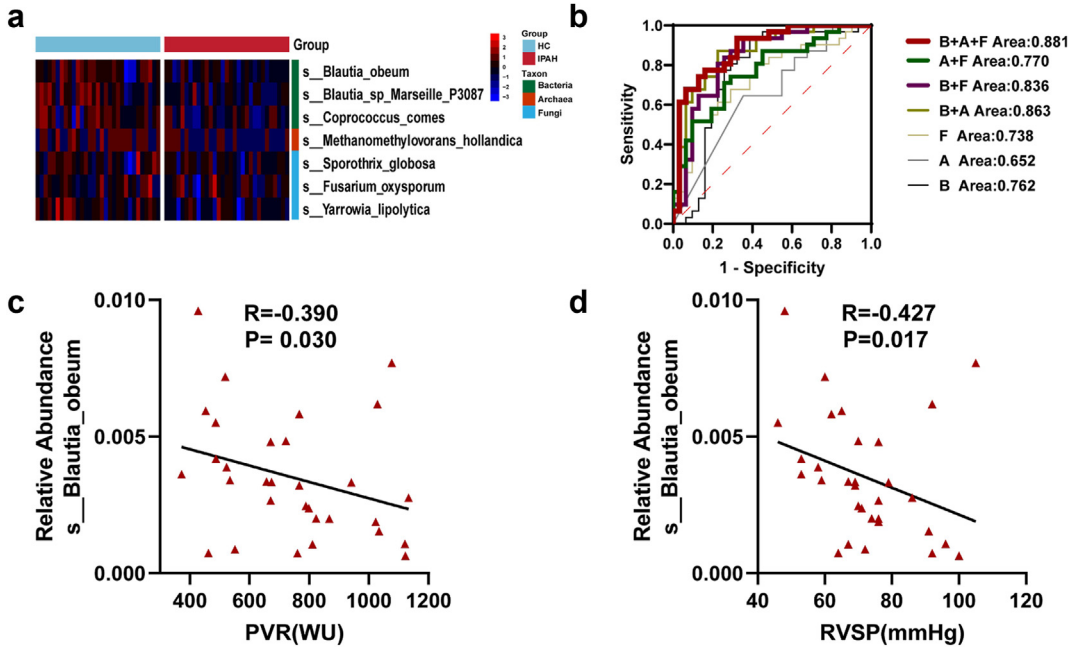

***Fig. 8:* Validation and diagnostic potential of dysbiotic microbiota in IPAH patients**. (**a**) Heat map showing clustering of different bacterial, archaeal, and fungal communities with their absolute abundances at the species level. These species exhibited consistent trends in both animal models and IPAH patients. (**b**) Receiver operating characteristic (ROC) curves using combinations of bacteria, archaea, fungi, bacteria + archaea, bacteria + fungi, archaea + fungi, and bacteria + archaea + fungi plotted for the diagnosis of IPAH, with the areas under the ROC curves (AUCs) calculated. (**c** and **d**) Scatter plots showing the relationship between significantly different microbiota and haemodynamic parameters in IPAH patients (n = 31). R represents the correlation coefficient.

community structure of IPAH. However, previous studies have predominantly concentrated on bacterial components of the GM, often neglecting the roles of archaea and fungi. This gap in the literature overlooks the significant contributions of these microbial communities to health and disease. In recent years, studies have begun to explore the roles of gut archaea and fungi, revealing their involvement in various metabolic pathways, immune responses, and inflammatory processes.[20–22]

While many archaea are known to thrive in extreme conditions, some mesophilic species have been discovered in the human gastrointestinal tract.[23] These stable commensals participate in processes such as trimethylamine metabolism, immune modulation, methanogenesis, and heavy-metal transformation.[24–27] In diseases such as colorectal cancer, Crohn disease, and asthma, shifts in archaeal populations have been documented.[28–30] For example, reduced diversity of archaea was found in patients with colorectal cancer, indicating involvement in tumorigenesis.[28] Another study suggested that certain archaea could serve as good indicators of the chronicity and activity of Crohn's disease.[29] These insights into the archaeal community's impact on metabolic and inflammatory processes provide a broader context for understanding their potential involvement in PAH.

Gut fungi, though less abundant than bacteria, play pivotal roles in maintaining gut health and contributing to disease.[31] They participate in regulating the host immune system and preserving the integrity of the gut barrier.[32] In other diseases, such as hypertension, coronary artery disease, and alcohol-associated liver disease, alterations in gut fungal communities have been observed.[33–35] These findings highlight the potential for gut fungi to influence inflammatory and metabolic pathways, which could also be relevant for PAH pathogenesis.

The induction of PAH phenotypes in recipient rats following FMT from IPAH patients or MCT-induced PAH rats confirms the association between GM dysbiosis and PAH. This experimental evidence supports previous observation of significant differences in gut bacterial structure between PAH patient populations and control groups, as well as between PAH animal models and their respective controls.[9,12,13,15,18]

Conversely, FMT from control rats significantly ameliorated PAH conditions in rat models, restoring GM composition and reversing PAH-associated changes in serum metabolite profiles. This aligns with previous studies that have shown the therapeutic potential of microbiota restoration in various diseases, such as hypertension, Parkinson's disease, and *Clostridioides difficile* infection.[36,37] In our study, the remission of FMT in PAH models indicates a similar potential for microbiota-based therapies in treating PAH; however, clinical trials are needed to validate these findings.

As expected, FMT therapy ameliorated gut bacterial, archaeal, and fungal dysbiosis in PAH rats. There were marked differences in the GM structure between the MCT and CON groups, while the microbiota of the NTM group resembled that of the CON group, indicating successful restoration of healthy GM through FMT. Correlations between the GM characteristics and haemodynamic and right-sided heart ultrasound indexes (RVSP, RVHI, PAAT, RVWT, and RVEED) underscore the significant role of the GM in PAH pathophysiology.

Our study demonstrated that FMT effectively modified the metabolic landscape disrupted in PAH, emphasizing the potential mechanisms by which the GM influence the disease progression. Previous research has shown that the GM influence disease progression through metabolic products that affect target organs.[38,39] Key metabolites, including lipids, organic acids, phenylpropanoids, and polyketides, were normalized by FMT. 5-Hydroxyindoleacetic acid (5-HIAA), known as the metabolic byproduct of 5-hydroxytryptamine, was significantly elevated in the MCT-PAH rats and was closely associated with the changes in gut microbial communities. Recent research has indicated that 5-HIAA can act as a ligand for GPR35, promoting the recruitment of neutrophils to inflammatory sites and thereby exerting proinflammatory effects.[40] The recruitment of inflammatory cells around pulmonary vasculature is another key pathological feature of IPAH. Proline, an amino acid and one of the metabolites in the intestine, plays a crucial role in the development of PAH.[41] It is essential for the formation of collagen, a major component of vascular structure. Alterations in collagen metabolism are fundamental to the vascular pathology of PAH. These findings suggest that FMT restores the GM and modulates metabolites to improve PAH symptoms.

The fundamental pathological mechanisms of PAH, including vascular remodelling, perivascular inflammation, and pulmonary vasoconstriction, are significantly regulated by FMT therapy, which affects the expression of relevant signalling pathways. The modulation of cytokine–cytokine receptor interaction, leucocyte transendothelial migration, and cell adhesion molecules suggests a potential reduction in inflammatory and vascular remodelling pathways.[42–44] FMT may help alleviate inflammatory cell infiltration and endothelial dysfunction, thereby reducing the inflammatory burden on pulmonary vasculature. Furthermore, the changes in pathways related to vascular smooth muscle contraction are particularly important, given that sustained vasoconstriction plays a critical role in PAH.[45] The impact of FMT on these signalling pathways suggests that it may lower pulmonary arterial pressure by alleviating vascular smooth muscle constriction, perivascular inflammation and vascular remodelling, thereby preventing the development of PAH. These findings further explore

the mechanisms through which the GM is involved in the development of PAH.

Seven microbial species exhibited consistent reductions in abundance in both PAH rodents and human patients. These include three bacterial species (*Blautia obeum*, *Blautia_sp Marseille P3087*, and *Coprococcus comes*), one archaeal species (*Methanomethylovorans hollandica*), and three fungal species (*Sporothrix globosa*, *Fusarium oxysporum*, and *Yarrowia lipolytica*). Using these seven multi-kingdom species, the AUC for diagnosing IPAH reached 0.881, demonstrating their potential diagnostic value.

Blautia obeum and *Blautia_sp Marseille P3087* belong to the *Blautia* genus, which plays a crucial role in maintaining GM balance and regulating inflammatory responses through the production of SCFAs.[46–49] Consistent with our findings, *Blautia obeum* has been shown to be less abundant in the GM of PAH patients compared with healthy controls.[12] Similarly, *Coprococcus comes*, a well-known butyrate-producing bacterium commonly found in the human gut,[50–52] was significantly reduced in both PAH patients and animal models in our study. Butyrate, a type of SCFA, has been shown to attenuate pulmonary vascular remodelling in hypoxia-induced PAH.[38] Therefore, the depletion of these SCFA-producing bacterial species may exacerbate PAH progression by promoting inflammation and vascular remodelling. The archaeal species *Methanomethylovorans hollandica* has not been studied in the context of PAH. However, archaea, particularly methanogens, are known to influence gut metabolic activity, which may contribute to systemic inflammation and metabolic dysregulation.[28,53,54] The fungal species *Sporothrix globosa*, *Fusarium oxysporum*, and *Yarrowia lipolytica* have not been extensively studied in the context of GM. Increasing interest in the gut mycobiome suggests that gut fungi may influence immune responses and inflammation, which are crucial factors in the development of PAH.[31] Further research into the gut mycobiome's influence on PAH could provide important insights into disease progression and potential therapeutic strategies.

This study makes several important contributions to the understanding of PAH pathogenesis and treatment. First, it establishes a direct association between GM dysbiosis and PAH, a link previously suggested but not empirically confirmed. Second, by incorporating archaea and fungi into the analysis, we provide a more comprehensive view of the GM's role in PAH. Finally, our findings on the therapeutic potential of FMT highlight a promising avenue for developing non-pharmacological treatments for PAH, emphasizing the need for further clinical investigations.

Despite the promising results, our study has several limitations. The small sample size from a single hospital in China and the use of animal models may limit the generalizability of the findings. Additionally, as diet significantly influences GM,[55] the lack of detailed dietary data from the participants is a clear limitation. Although there were no differences in dietary patterns in our study, we recognize that future studies incorporating detailed nutritional analyses (e.g., macronutrient and micronutrient composition) will be essential to account for dietary influences and further clarify the relationship between gut microbiota dysbiosis and PAH. Third, the fold change threshold of >2 used in the RNA-sequencing analysis, although commonly applied in similar studies,[56,57] is somewhat arbitrary and may overlook smaller yet potentially relevant changes in gene expression. Future studies should validate these findings through large-scale, multicenter trials, incorporate detailed dietary assessments, and investigate the mechanistic pathways of GM in PAH, including the roles of specific microbial species and their metabolites, to uncover targeted therapeutic strategies.

Conclusion

In this study, we underscored for the first time the critical role of multi-kingdom GM, including bacteria, archaea, and fungi, in the pathogenesis and treatment of PAH. More importantly, we showed the therapeutic potential of FMT in reversing PAH phenotypes. Thus, more attention should be paid to the microbial underpinnings of PAH and the therapeutic potential of targeted multi-kingdom microbiota–based interventions. This study opens up new avenues for developing innovative microbiota-based therapies, offering new hope for patients with this debilitating condition.

Contributors

Substantial contributions to the conception or design of the work: X.L., Y.C., J.Z., Z.T.; the acquisition, analysis: Y.C., Z.C., J.L., X.Z.; interpretation of data for the work: Y.C., L.M., B.X.; Draughting the work or reviewing it critically for important intellectual content: W.Y.; L.F.; Y.J., Z.F., P.S.; Final approval of the version to be published: all authors.; Agreement to be accountable for all aspects of the work in ensuring that questions related to the accuracy or integrity of any part of the work are appropriately investigated and resolved: Y.C., Z.C., L.L., J.L., T.Z., J.Z., X.L.

Data sharing statement

Metagenomics raw sequences were deposited in the NCBI Sequence Read Archive under accession number PRJNA1127260 for human and PRJNA1126667 and PRJNA1205488 for rats. Metagenomics raw sequences were deposited in the MetaboLights under accession number MTBLS10563.[58] These RNA-seq sequence data have been submitted to the GEO databases under accession number GSE271297.

Declaration of interests

The authors declare no conflict of interest.

Acknowledgements

We thank LetPub (www.letpub.com.cn) for its linguistic assistance during the preparation of this manuscript. All Schematic overviews and graphical abstract were created by Figdraw (www.figdraw.com). This work was supported by Noncommunicable Chronic Diseases-National Science and Technology Major Projects No. 2024ZD0531200, No. 2024ZD0531201 (Research on Prevention and Treatment of Cancer, Cardiovascular and Cerebrovascular Diseases, Respiratory Diseases, and Metabolic Diseases), the National Natural Science Foundation of China

(No. 82170302, 82370432), Financial Budgeting Project of Beijing Institute of Respiratory Medicine (Ysbz2025004, Ysbz2025007), National clinical key specialty construction project Cardiovascular Surgery, Reform and Development Program of Beijing Institute of Respiratory Medicine (Ggyfz202417, Ggyfz202501), Clinical Research Incubation Program of Beijing Chaoyang Hospital Affiliated to Capital Medical University (CYFH202209).

Appendix A. Supplementary data

Supplementary data related to this article can be found at https://doi.org/10.1016/j.ebiom.2025.105686.

References

1 Maron BA, Abman SH, Elliott CG, et al. Pulmonary arterial hypertension: diagnosis, treatment, and novel advances. *Am J Resp Crit Care*. 2021;203:1472–1487.
2 Hoeper MM, Pausch C, Grunig E, et al. Idiopathic pulmonary arterial hypertension phenotypes determined by cluster analysis from the COMPERA registry. *J Heart Lung Transpl*. 2020;39:1435–1444.
3 Yang Y, Zhang H, Wang Y, et al. Promising dawn in the management of pulmonary hypertension: the mystery veil of gut microbiota. *Imeta*. 2024;3:e159.
4 Yan Q, Li S, Yan Q, et al. A genomic compendium of cultivated human gut fungi characterizes the gut mycobiome and its relevance to common diseases. *Cell*. 2024;187:2969–2989.
5 Chibani CM, Mahnert A, Borrel G, et al. A catalogue of 1,167 genomes from the human gut archaeome. *Nat Microbiol*. 2022;7:48–61.
6 Pennisi E. Survey of archaea in the body reveals other microbial guests. *Science*. 2017;358:983.
7 Duan JL, He HQ, Yu Y, et al. E3 ligase c-Cbl regulates intestinal inflammation through suppressing fungi-induced noncanonical NF-kappaB activation. *Sci Adv*. 2021;7:eabe5171.
8 Doron I, Leonardi I, Li XV, et al. Human gut mycobiota tune immunity via CARD9-dependent induction of anti-fungal IgG antibodies. *Cell*. 2021;184:1017–1031.
9 Kim S, Rigatto K, Gazzana MB, et al. Altered gut microbiome profile in patients with pulmonary arterial hypertension. *Hypertension*. 2020;75:1063–1071.
10 Jose A, Apewokin S, Hussein WE, Ollberding NJ, Elwing JM, Haslam DB. A unique gut microbiota signature in pulmonary arterial hypertension: a pilot study. *Pulm Circ*. 2022;12:e12051.
11 Ikubo Y, Sanada TJ, Hosomi K, et al. Altered gut microbiota and its association with inflammation in patients with chronic thromboembolic pulmonary hypertension: a single-center observational study in Japan. *BMC Pulm Med*. 2022;22:138.
12 Moutsoglou DM, Tatah J, Prisco SZ, et al. Pulmonary arterial hypertension patients have a Proinflammatory gut microbiome and altered circulating microbial metabolites. *Am J Resp Crit Care*. 2023;207:740–756.
13 Callejo M, Mondejar-Parreño G, Barreira B, et al. Pulmonary arterial hypertension affects the rat gut microbiome. *Sci Rep*. 2018;8:9610–9681.
14 Gheblawi M, Wang K, Oudit GY. ACE2 (Angiotensin-Converting Enzyme 2)-mediated protection from pulmonary hypertension. *Hypertension*. 2020;76:28–29.
15 Hong W, Mo Q, Wang L, et al. Changes in the gut microbiome and metabolome in a rat model of pulmonary arterial hypertension. *Bioengineered*. 2021;12:5173–5183.
16 Luo Y, Teng X, Zhang L, et al. CD146-HIF-1α hypoxic reprogramming drives vascular remodeling and pulmonary arterial hypertension. *Nat Commun*. 2019;10.
17 Xiong PY, Motamed M, Chen KH, et al. Inhibiting pyruvate kinase muscle isoform 2 regresses group 2 pulmonary hypertension induced by supra-coronary aortic banding. *Acta Physiol (Oxf)*. 2022;234(2):e13764.
18 Sanada TJ, Hosomi K, Shoji H, et al. Gut microbiota modification suppresses the development of pulmonary arterial hypertension in an SU5416/hypoxia rat model. *Pulm Circ*. 2020;10:1365052046–1765618565.
19 Wang Y, Yan Z, Luo S, et al. Gut microbiota-derived succinate aggravates acute lung injury after intestinal ischaemia/reperfusion in mice. *Eur Respir J*. 2023;61:2200840.
20 Hoegenauer C, Hammer HF, Mahnert A, Moissl-Eichinger C. Methanogenic archaea in the human gastrointestinal tract. *Nat Rev Gastroenterol Hepatol*. 2022;19:805–813.
21 Lane MA, Neary D, Cooper GM. Activation of a cellular transforming gene in tumours induced by Abelson murine leukaemia virus. *Nature*. 1982;300:659–661.
22 Mahmoudi E, Mozhgani SH, Sharifinejad N. The role of mycobiota-genotype association in inflammatory bowel diseases: a narrative review. *Gut Pathog*. 2021;13:31.
23 Eme L, Spang A, Lombard J, Stairs CW, Ettema T. Archaea and the origin of eukaryotes. *Nat Rev Microbiol*. 2017;15:711–723.
24 Lurie-Weinberger MN, Gophna U. Archaea in and on the human body: health implications and future directions. *Plos Pathog*. 2015;11:e1004833.
25 Brugere JF, Borrel G, Gaci N, Tottey W, O'Toole PW, Malpuech-Brugere C. Archaebiotics: proposed therapeutic use of archaea to prevent trimethylaminuria and cardiovascular disease. *Gut Microbes*. 2014;5:5–10.
26 Blais LP, Marsolais D, Cormier Y, et al. Increased prevalence of Methanosphaera stadtmanae in inflammatory bowel diseases. *PLoS One*. 2014;9:e87734.
27 Eckburg PB, Lepp PW, Relman DA. Archaea and their potential role in human disease. *Infect Immun*. 2003;71:591–596.
28 Coker OO, Wu W, Wong SH, Sung J, Yu J. Altered gut archaea composition and interaction with bacteria are associated with colorectal cancer. *Gastroenterology*. 2020;159:1459–1470.
29 Krawczyk A, Gosiewski T, Zapala B, Kowalska-Duplaga K, Salamon D. Alterations in intestinal Archaea composition in pediatric patients with Crohn's disease based on next-generation sequencing - a pilot study. *Gut Microbes*. 2023;15:2276806.
30 Barnett D, Mommers M, Penders J, Arts I, Thijs C. Intestinal archaea inversely associated with childhood asthma. *J Allergy Clin Immunol*. 2019;143:2305–2307.
31 Zhang F, Aschenbrenner D, Yoo JY, Zuo T. The gut mycobiome in health, disease, and clinical applications in association with the gut bacterial microbiome assembly. *Lancet Microbe*. 2022;3:e969–e983.
32 Zhang L, Zhan H, Xu W, Yan S, Ng SC. The role of gut mycobiome in health and diseases. *Therap Adv Gastroenterol*. 2021;14:1088230106.
33 Zou Y, Ge A, Lydia B, Huang C, Wang Q, Yu Y. Gut mycobiome dysbiosis contributes to the development of hypertension and its response to immunoglobulin light chains. *Front Immunol*. 2022;13:1089295.
34 An K, Jia Y, Xie B, et al. Alterations in the gut mycobiome with coronary artery disease severity. *eBioMedicine*. 2024;103:105137.
35 Zeng S, Rosati E, Saggau C, et al. Candida albicans-specific Th17 cell-mediated response contributes to alcohol-associated liver disease. *Cell Host Microbe*. 2023;31:389–404.
36 Zhong HJ, Zeng HL, Cai YL, et al. Washed microbiota transplantation lowers blood pressure in patients with hypertension. *Front Cell Infect Microbial*. 2021;11:679624.
37 Cheng Y, Tan G, Zhu Q, et al. Efficacy of fecal microbiota transplantation in patients with Parkinson's disease: clinical trial results from a randomized, placebo-controlled design. *Gut Microbes*. 2023;15:2284247.
38 Karoor V, Strassheim D, Sullivan T, et al. The short-chain fatty acid butyrate attenuates pulmonary vascular remodeling and inflammation in hypoxia-induced pulmonary hypertension. *Int J Mol Sci*. 2021;22:9916.
39 Jiang S, Shui Y, Cui Y, et al. Gut microbiota dependent trimethylamine N-oxide aggravates angiotensin II–induced hypertension. *Redox Biol*. 2021;46:102115.
40 De Giovanni M, Tam H, Valet C, Xu Y, Looney MR, Cyster JG. GPR35 promotes neutrophil recruitment in response to serotonin metabolite 5-HIAA. *Cell*. 2022;185:815–830.
41 Wertheim BM, Wang RS, Guillermier C, et al. Proline and glucose metabolic reprogramming supports vascular endothelial and medial biomass in pulmonary arterial hypertension. *JCI Insight*. 2023;8:e163932.
42 Schimmel L, van der Stoel M, Rianna C, et al. Stiffness-induced endothelial DLC-1 expression forces leukocyte spreading through stabilization of the ICAM-1 adhesome. *Cell Rep*. 2018;24:3115–3124.
43 Yaku A, Inagaki T, Asano R, et al. Regnase-1 prevents pulmonary arterial hypertension through mRNA degradation of interleukin-6 and platelet-derived growth factor in alveolar macrophages. *Circulation*. 2022;146:1006–1022.

44 Sun M, Ishii R, Okumura K, et al. Experimental right ventricular hypertension induces regional beta1-integrin-mediated transduction of hypertrophic and profibrotic right and left ventricular signaling. *J Am Heart Assoc*. 2018;7:e007928.
45 Bussone G, Tamby MC, Calzas C, et al. IgG from patients with pulmonary arterial hypertension and/or systemic sclerosis binds to vascular smooth muscle cells and induces cell contraction. *Ann Rheum Dis*. 2012;71:596–605.
46 Montgomery TL, Toppen LC, Eckstrom K, et al. Lactobacillaceae differentially impact butyrate-producing gut microbiota to drive CNS autoimmunity. *Gut Microbes*. 2024;16(1):2418415.
47 Zhao Z, Li C, Huang J, et al. Phlorizin limits bovine viral diarrhea virus infection in mice via regulating gut microbiota composition. *J Agric Food Chem*. 2024;72(17):9906–9914.
48 Mei X, Li Y, Zhang X, et al. Maternal phlorizin intake protects offspring from maternal obesity-induced metabolic disorders in mice via targeting gut microbiota to activate the SCFA-GPR43 pathway. *J Agric Food Chem*. 2024;72(9):4703–4725.
49 Rodriguez-Garcia A, Arroyo A, García-Vicente R, et al. Short-chain fatty acid production by gut microbiota predicts treatment response in multiple Myeloma. *Clin Cancer Res*. 2024;30(4):904–917.
50 Pan X, Kaminga AC, Liu A, Wen SW, Luo M, Luo J. Gut microbiota, glucose, lipid, and water-electrolyte metabolism in children with nonalcoholic fatty liver disease. *Front Cell Infect Microbiol*. 2021;11:683743.
51 Abdugheni R, Wang WZ, Wang YJ, et al. Metabolite profiling of human-originated Lachnospiraceae at the strain level. *Imeta*. 2022;1(4):e58.
52 Sambruni G, Macandog AD, Wirbel J, et al. Location and condition based reconstruction of colon cancer microbiome from human RNA sequencing data. *Genome Med*. 2023;15(1):32.
53 Li T, Coker OO, Sun Y, et al. Multi-cohort analysis reveals altered archaea in colorectal cancer fecal samples across populations. *Gastroenterology*. 2024;168:525–538.
54 Borrel G, McCann A, Deane J, et al. Genomics and metagenomics of trimethylamine-utilizing Archaea in the human gut microbiome. *ISME J*. 2017;11(9):2059–2074.
55 Perler BK, Friedman ES, Wu GD. The role of the gut microbiota in the relationship between diet and human health. *Annu Rev Physiol*. 2023;85:449–468.
56 Simon EP, Freije CA, Farber BA, et al. Transcriptomic characterization of fibrolamellar hepatocellular carcinoma. *Proc Natl Acad Sci U S A*. 2015;112(44):E5916–E5925.
57 Illescas O, Ferrero G, Belfiore A, et al. Modulation of faecal miRNAs highlights the preventive effects of a Mediterranean low-inflammatory dietary intervention. *Clin Nutr*. 2024;43(4):951–959.
58 Yurekten O, Payne T, Tejera N, et al. MetaboLights: open data repository for metabolomics. *Nucleic Acids Res*. 2024;52:D640–D646.